Conformable metal oxide platelets – A smart surface armor for green tribology

Hendrik M. Reinhardt [a,*], Petr Chizhik [b], Dirk Dietzel [b,c], Hee-Cheol Kim [a], Michael Dasbach [a], André Schirmeisen [b,c,**], Norbert Hampp [a]

[a] *Institute of Physical Chemistry, Philipps-Universität Marburg, 35043 Marburg, Germany*
[b] *Institute of Applied Physics, Justus-Liebig-Univerity Giessen, Heinrich-Buff-Ring 16, D-35392 Giessen, Germany*
[c] *Center for Materials Research, Justus-Liebig-Universität, 35392 Gießen, Germany*

ARTICLE INFO

ABSTRACT

The reduction of friction and wear is a crucial performance criterion for most technical processes. This is particularly true for the ubiquitous case of oil lubricated machinery made from steel components. Here we introduce a facile laser treatment that significantly enhances the tribological performance of bearing steel 100Cr6, a material widely used for the manufacture of ball and roller bearings. By applying repeated nanosecond-pulses of focussed laser-beam irradiation under ambient air, a surface-protective tribo-layer is generated by a method that exploits self-organization for the formation of conformable metal oxide platelets consisting of vertically aligned transition metal oxides nanorods on the steel substrate. These submicron-sized metal oxide platelets protect the surfaces similar to scale armor and the tribological performance of the bearing steel 100Cr6 was significantly enhanced. Based on laboratory tests using a rotational pin-on-disk trib- ometer under oil lubricated conditions, close to zero wear with simultaneous reduction of friction by 54% was achieved. Even under the harsh conditions in the pin-on-disk tribometer these metal oxide platelets turn out to be remarkably robust against detachment and crumbling for lasting millions of cycles at a slip rate of 100%. The origin of this resilience is based on a special substructure of the platelets that, counter-intuitively for ceramic material, enables shape adaptations to surface deformations emergent upon high mechanical stress.

1. Introduction

For economic and ecologic reasons, the reduction of friction and wear in technological systems has become a topic of ever increasing importance [1–3]. In this context, especially oil lubricated machinery plays an important role, since components like gear boxes and bearings are ubiquitous in essential sectors such as transportation, production and energy generation. In order to improve the performance of such systems, there are basically two approaches that can be applied.

One approach is to focus on the lubricants. But due to their long history of development, lubricants are already highly optimized for almost every application and available at industrial scales. Improvement potentials are therefore found rather in the admixture of application-specific additives. Besides using well known additives like zinc dia-lkyldithiophosphate (ZDDP) [4,5], molybdenum dithiocarbamates (MoDTC) [6], and MoS$_2$ [6], new approaches are currently evolving that

include materials like e.g. nanoparticles [6,7], phyllosilicates [8–11], or graphene [12–14] as well as new concepts like e.g superlubricity [7, 15–17].

An alternative approach, that offers potential for optimization, is on the other hand the surface modification of the metal components used in a lubricated environment. Here, the tribological suitability depends to a large extent on factors such as surface roughness and hardness, as well as the wettability of surfaces with lubricants. Although some additives allow for an in-situ-modification of the surfaces [5,11] the general approach is surface modification during the production stage. For instance, hard coatings like DLC films can be applied to improve tribo- logical properties [18–24]. However, techniques for applying hard coatings such as chemical or physical vapor deposition (CVD or PVD) [25] are associated with high acquisition and operating costs which limits their economic use to special applications. By contrast, the inte- gration of laser-based processes is comparatively favorable, since costs
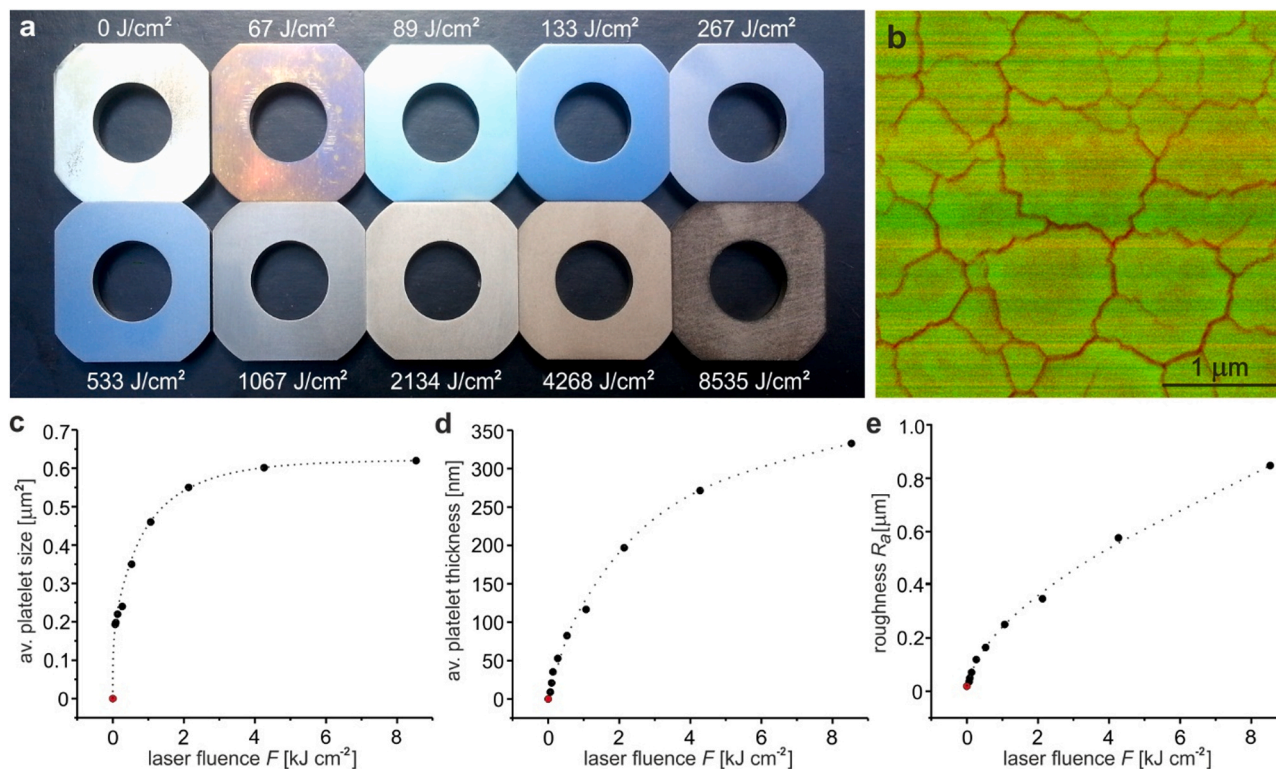

Fig. 1. Formation of metal oxide platelets on 100Cr6 bearing steel. (a) Set of 10 bearing steel samples (100Cr6, edge length 2 cm) for tribological evaluation. Laser fluences F applied for respective surface modifications are indicated for each sample. (b) Electron micrograph of metal oxide platelets on bearing steel modified with $F = 2134$ Jcm^{-2}. (c) Statistical analysis of the average surface area of metal oxide platelets in dependence on the laser fluence. (d) Average platelet thickness as well as root mean square roughness (e) versus the laser fluence applied for surface modification.

for integration and operation are significantly lower. Laser micromachining already developed into a well-established method for the generation of lubrication pockets or rather surface patterns facilitating the transport of lubricants to required positions [26,27]. In addition to that, intense laser irradiation is used to adapt the interfacial shear stress distribution of materials to specific tribological requirements [28–33].

From the viewpoint of practical applicability, a fast and robust laser process running under ambient conditions is a worthwhile goal. As such, the objective of this study was the investigation of laser-induced surface modifications in ambient air. Friction-reducing effects of laser-generated metal oxide films on steel have already been reported though their origin is not fully understood yet [34,35]. Oxide films are commonly recognized as suppressors of welding bridges between friction pairs, thus resembling a factor that improves tribological behavior. However, the susceptibility of metal oxide films against mechanical stress appears to be a major hurdle for practical applications [36].

The present study shows that this limitation with respect to long term mechanical stability can be overcome by a laser process that utilizes self-organization for the generation of hierarchically structured metal oxides. Chromium steel 100Cr6, a material frequently applied for the manufacture of ball and roller bearings, is used for demonstration purposes. The formation of metal oxides on 100Cr6 was induced by photothermal heating with a nanosecond pulsed laser. Depending on the energy input per unit area, henceforth referred to as laser fluence *F*, 100Cr6 steel shows intriguing transformations of its tribological characteristics: Surface modification with $F = 67$ Jcm^{-2} resulted in friction reduced by 90% while a laser fluence of $F = 1067$ Jcm^{-2} yields about 50% reduction of friction combined with close to zero wear. The observed effects originate from submicron platelets which consist of vertically aligned transition metal oxides nanorods that cover the surface of laser modified 100Cr6 similar to scale armor.

2. Results and discussion

The impact of pulsed laser modification on the tribological properties of 100Cr6 was analyzed on a series of 10 samples. Surface modifications were conducted with a frequency-doubled Nd:YVO4 laser ($\lambda = 532$ nm) emitting nanosecond pulses (6 ns) with an energy of 32 μJ at a frequency of 50 kHz. The laser beam was focused to a spot of 30 μm diameter ($1e^{-2}$) and scanned with variable speeds thus subjecting each of the 10 samples to a different laser fluence F. Irradiations were carried out in ambient air and are therefore accompanied by oxidation, as annealing colors on laser modified 100Cr6 samples show (Fig. 1a). A detailed description of the laser-induced oxidization process is provided in a previous publication [37].

In short, the irradiation of steel under given conditions leads to surface melting. Liquid thin films are intrinsically unstable thus transforming into thermodynamically more favorable geometries in a process called dewetting. In the present case, this leads to the formation of nanometer-sized droplets which simultaneously oxidize due to contact with air. The resulting metal oxides do not cover the surface of 100Cr6 as a film, but rather form closely packed platelets divided by gaps of a few tens of nanometers (Fig. 1b). Cracks are caused by the rapid heating and cooling cycles that occur when the laser spot is scanned over 100Cr6. Since the coefficients of thermal expansion are not identical for the steel and its oxides, rapid thermal cycling induces distortion stress which causes crack formation. This is apparent by a dependence found between the speed at which the laser spot is scanned across steel samples and the average size of resulting metal oxide platelets (Fig. 1c). High scan speeds, which are synonymous with low laser fluences, lead to the formation of smaller platelets compared to low scan speeds. A saturation behavior of this dependence is observed for laser fluences exceeding 2 kJcm^{-2}. In general, the variation of laser spot scan speeds facilitates the adjustment of platelet sizes in a range of 0.2–0.6 μm^2. Similarly, the
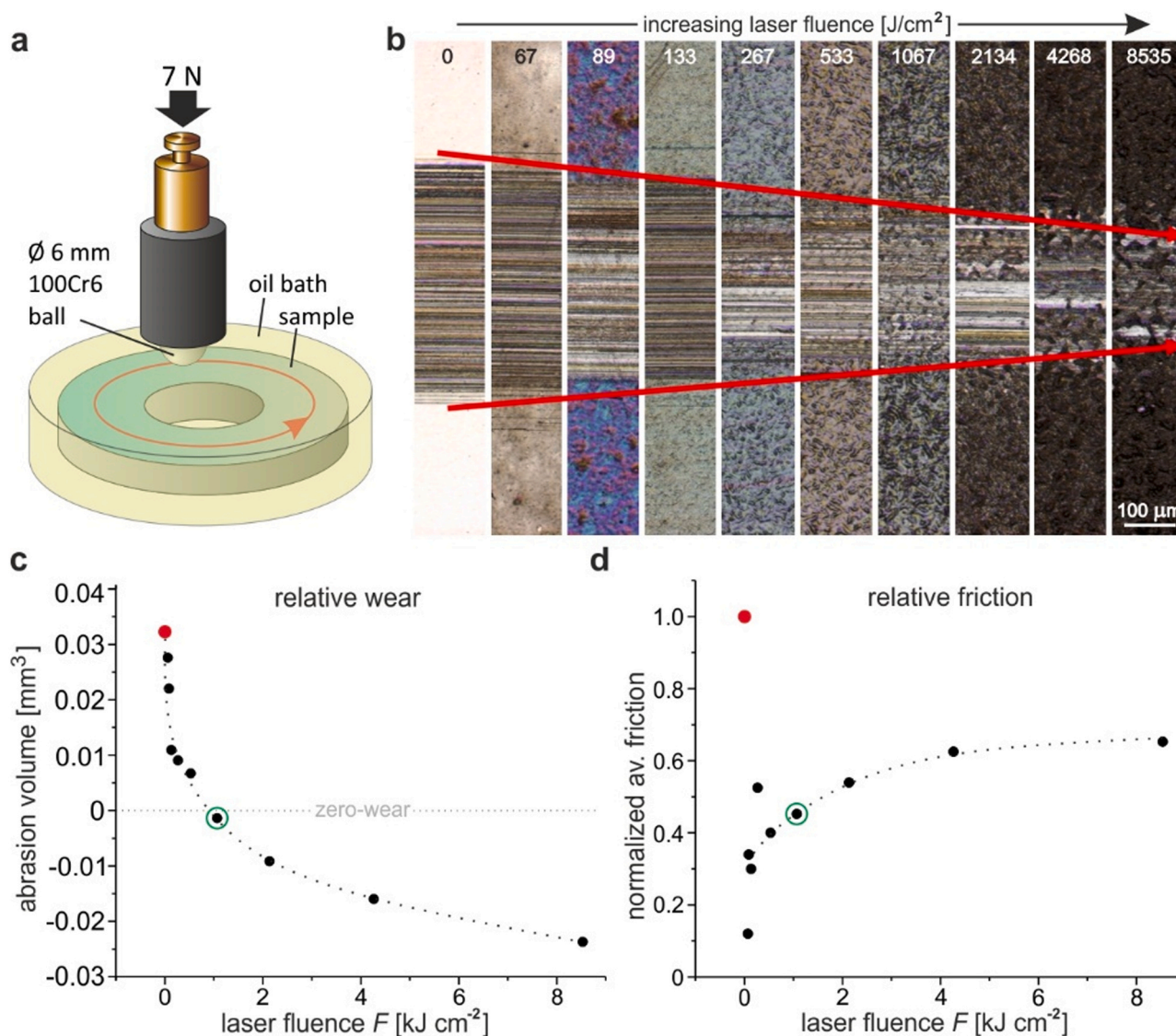
Fig. 2. Tribological evaluation of laser-modified 100Cr6 bearing steel. (a) Schematic representation of the ball-on-disk-tribometer used for tribological tests. (b) Optical micrographs of wear tracks induced by tribological tests (c) Absolute abrasion volume of laser modified 100Cr6 samples in comparison to an unmodified 100Cr6 reference sample (red dot). (d) Relative friction of laser modified 100Cr6 samples in comparison to unmodified 100Cr6 (reference marked in red and normalized to 1). (For interpretation of the references to colour in this figure legend, the reader is referred to the web version of this article.)

thickness of metal oxides generated by pulsed laser treatment of 100Cr6 is tunable by means of the applied laser fluence Fig. 1d). Starting from the natural passivation layer of the steel, metal oxides up to a thickness of 340 nm were created within the frame of this screening. In addition to this, the surface roughness of laser modified 100Cr6 samples was analyzed. All roughness values have been determined as root mean square roughness R_a shown in Fig. 1e. Surface roughnesses are consistently rising with increasing laser fluence.

The analysis of tribological properties was conducted using a pin-on-disk tribometer schematically displayed in Fig. 2a [11,38]. 100Cr6 ball bearing balls with a diameter of 6 mm served as counterbodies against laser modified 100Cr6 substrates. A constant load of 7 N was applied in the contact between the ball and the disk. All measurements were conducted under lubrication with standard commercial gear oil (Castrol X320) at a constant temperature of 70 °C. Friction forces were permanently recorded while spinning the steel ball at a constant rotational speed of 2500 rpm which equals a sliding speed of appr. 2 ms^{-1}. Under these conditions, each sample was tested for 23 h which results in 3.45 million revolutions or rather a total sliding distance of 165 km.

After a run-in period of 1–2 h, the interfacial friction remained

essentially unchanged for the residual duration of tribological tests with a friction coefficient of appr. $\mu = 0.045$ for the untreated steel surfaces (see Supporting Information for details). Wear scars induced by the tribological tests are shown in Fig. 2b. Please note, that to some extend the quantification of these wear scars can also include plastic deformation of the metal substrate. Nonetheless, steady decreases of the wear scar widths indicate improving resistance to wear with increasing laser fluence *F*. It is noticeable that samples treated with laser fluences below 1 kJcm^{-2} show typical stripe patterns whereas those exposed to higher doses rather show rugged wear tracks. Investigations with white light interferometry (see Appendix C and Supporting Information for details) revealed significant differences in the overall wear behavior across the sample set (Fig. 2c).

Samples modified with laser fluences below 1 kJcm^{-2} generally show abrasion, whereas abrasion volumes are negative for samples subjected to laser treatments exceeding 1 kJcm^{-2}. The latter implicates material deposits on samples during pin-on-disk-testing. Abrasion marks observed on steel balls used as counterbodies for respective test runs disclose the source of the deposited material. It is thus evident that 100Cr6 bearing steel modified with laser fluences exceeding 1 kJcm^{-2}
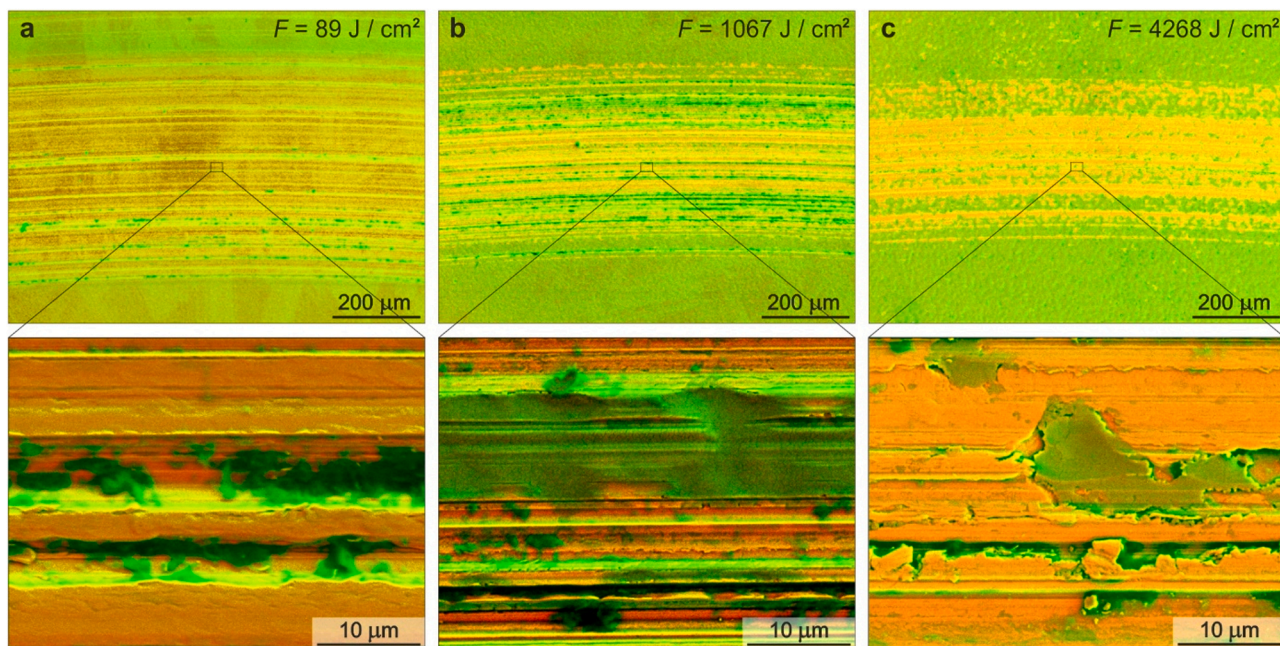
Fig. 3. Wear track morphology of laser-modified bearing steel. SEM inspection of wear tracks on 100Cr6 laser-modified with $F = 89$ Jcm^{-2}(a), $F = 1067$ Jcm^{-2} (b), and $F = 4268$ Jcm^{-2} (c). Metals are contrasted in orange whereas metal oxides are green, based on results from backscattered electron detection. (For interpretation of the references to colour in this figure legend, the reader is referred to the web version of this article.)

appears to be more abrasion resistant than its untreated counterpart. Although the overall wear of the steel spheres seems to be higher for smaller irradiation doses, as evidenced by the wear track width, effective material transfer to the substrate mostly occurs for higher irradiation doses which coincide with a higher surface roughness.

Practically wear-free bearing steel 100Cr6 can be obtained when a laser fluence of appr. 1 kJcm^{-2} is applied for surface treatment, as the corresponding sample marked with a green circle demonstrates (Fig. 2c). Besides total wear, the average friction was determined for each sample based on data obtained from pin-on-disk experiments. Fig. 2d shows average friction values for all laser modified samples in relative comparison to untreated 100Cr6 steel (red point). More specifically, for the data shown in Fig. 2d, friction values for all samples have first been calculated as the average friction over 20 h after a run-in time of 3 h (see Supporting Information, Fig. S2.1). Each of these values has then been divided by the average friction of the untreated steel sample.

It is striking, that the lowest irradiation dose applied for surface modification ($F = 67$ kJcm^{-2}) results in an almost 90% reduction of relative friction. Samples exposed to laser fluences in the range of 89–267 Jcm^{-2} show an upward trend of relative friction which is characterized by distinct dispersion. Further increases of laser fluence lead to a steady rise running into saturation on a level of about 35% friction reduction compared to untreated 100Cr6. The virtually wear-free sample (marked with a green circle in Fig. 2c and 2d) falls into this regime and shows a reduction of friction exceeding 50% compared to untreated 100Cr6.

From a practical point of view, this very combination is considered ideal, whilst higher reductions of friction may be achieved. It must, however, be noted that the susceptibility of laser-generated metal oxide platelets to mechanical damage depends on their thickness. An electron micrograph of the wear track on a sample modified with $F = 89$ Jcm^{-2} shows that metal oxide platelets of only 25 nm thickness are seriously damaged during pin-on-disk testing (Fig. 3a). In contrast to that, metal oxide platelets featuring 120 nm thickness ($F = 1067$ Jcm^{-2}) still cover extended surface areas of the bearing steel after pin-on-disk testing (Fig. 3b). Further increases of F result in metal oxides that are almost unaffected by attrition upon pin-on-disk testing. Metal abrasion from

100Cr6 steel ball counterbodies covers the wear track of 100Cr6 modified with $F = 4268$ Jcm^{-2} (ca. 275 nm oxide thickness) as the SEM inspection shows (Fig. 3c).

From a tribological point of view, neither negative nor positive abrasion volumes are desirable as both indicate wear of at least one part of a friction pair. Consequently, a zero-wear behavior, as observed for 100Cr6 treated with $F = 1067$ Jcm^{-2}, is of great interest specifically in the given case of concomitant friction reduction by 54% (green circles in Fig. 2c,d).

The origin of these unusual tribological properties has been investigated: Electron micrographs illustrated in Fig. 4a–d show that the wear track of 100Cr6 modified with $F = 1067$ Jcm^{-2} is predominantly covered with metal oxide platelets. Even in mechanically stressed areas, abrasion does not necessarily occur, but rather the platelets adapt to morphological changes such as scratches engraved by the steel ball counterbody. Considering that metal oxides are usually associated with properties such as hardness and brittleness, the observed plastic deformations of laser generated-metal oxide platelets are quite astonishing. They are warping around sharp edges and corners of newly created morphologies without exposing the metal substrate (Fig. 4b,c).

Cracking and crumbling of the platelets seems to occur only under excessive distortion. The origin for this flexibility was found in a special substructure that can be described as an array of vertically aligned metal oxide nanorods (Fig. 4e,f). For 100Cr6 modified with $F = 1067$ Jcm^{-2}, the diameters of these nanorods vary in a range between 10 and 100 nm while their lengths show a narrow distribution around 120 nm. Due to the conical shape of these nanorods, the platelets, which resemble nanorod arrays, can bend out of their initially planar geometry without building up destructive mechanical stress (Fig. 4g). A platelet hanging down from an edge similar to Salvatore Dali's "Melting Clocks" provides an exemplary demonstration of mechanically unimpeded bending (Fig. 4h). This extraordinary flexibility ensures the longevity of laser-generated metal oxide platelets. Moreover, the hierarchical structure of metal oxide platelets promotes wettability with lubricants as the AFM topography displayed in Fig. 4i suggests. Cracks between the platelets resemble lubricant pockets and the platelets themselves feature nano-structured surfaces thus stabilizing lubricant films. More specifically, the cracks between oxide platelets (see Figs. 1b and 4i) can keep minute
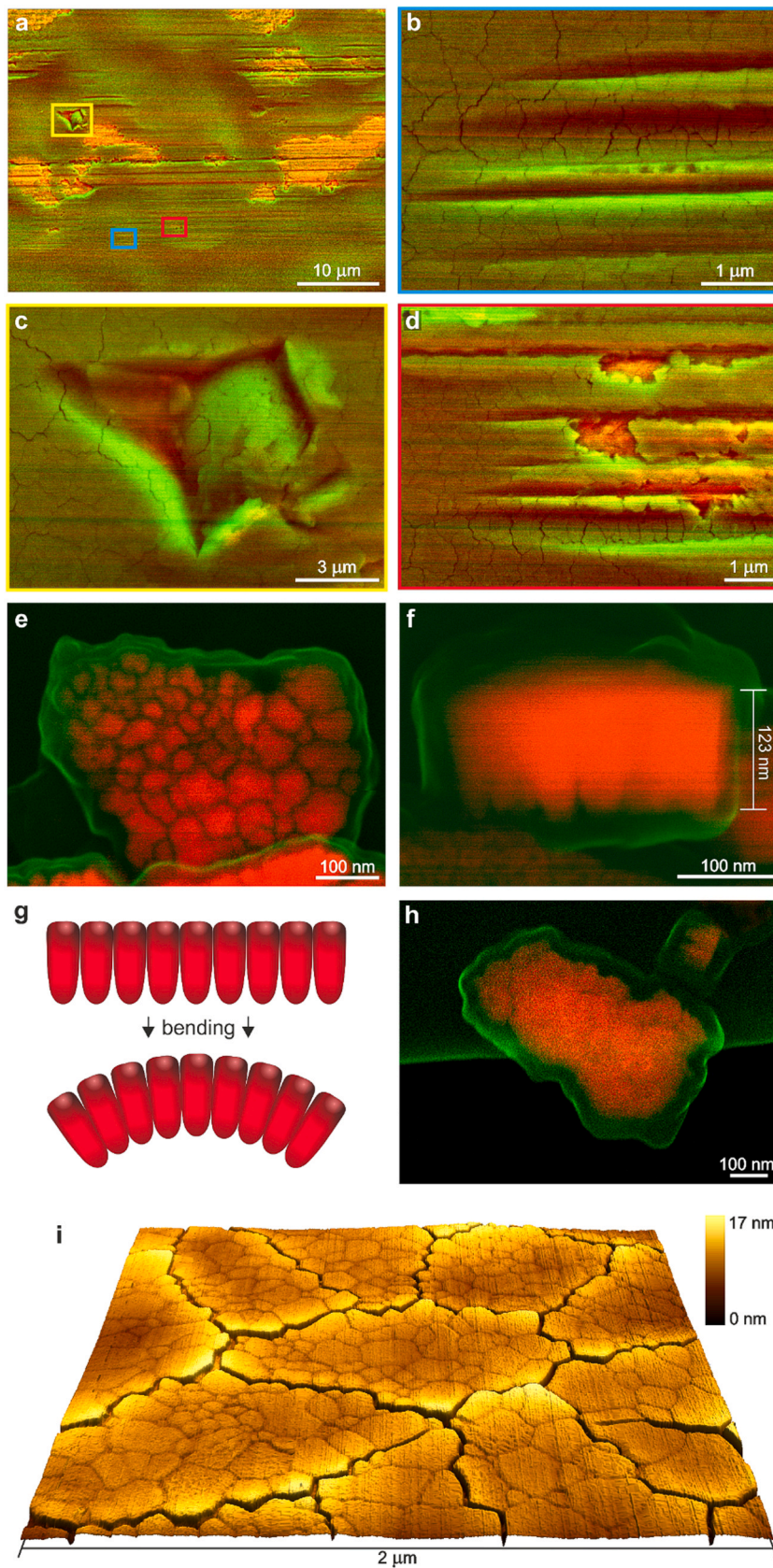
Fig. 4. Origin of the tribological performance of laser generated metal oxide platelets. (a) SEM inspection of a wear track on bearing steel 100Cr6 modified with a fluence of $F = 1067\ \mathrm{Jcm}^{-2}$. Metal oxides are contrasted in green whereas the underlying steel contrasts in orange. (b–d) Detailed views on areas marked by respective color frames in (a). (e, f) SEM image of a single metal-oxide platelet ($F = 1067\ \mathrm{Jcm}^{-2}$) revealing a substructure of vertically aligned nanorods. (g) Schematic representation of bending or rather shape adaption of a nanorod array. (h) A nanorod-array hanging down over the edge of a carbon thin film. (i) AFM topography of 100Cr6 modified with $F = 1067\ \mathrm{Jcm}^{-2}$. (For interpretation of the references to colour in this figure legend, the reader is referred to the web version of this article.)
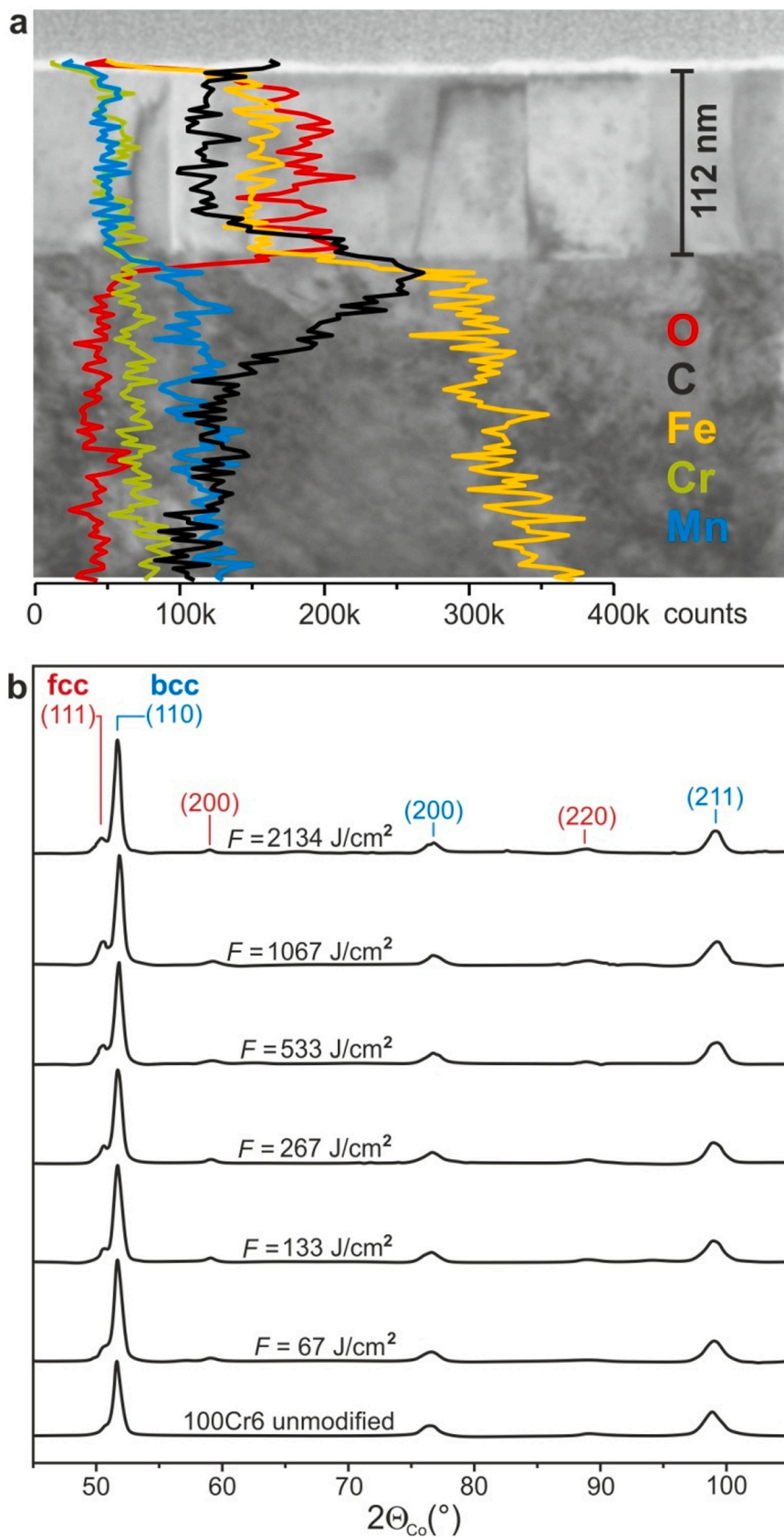
Fig. 5. Composition and structure of laser modified 100Cr6. (a) Cross-sectional view on 100Cr6 modified with $F = 1067$ Jcm^{-2} (prepared by focused ion beam (FIB) milling). Colored lines provide information about the local composition obtained via energy dispersive x-ray analysis (EDX). (b) X-ray diffractograms of 100Cr6 samples modified with different laser fluences F in relation to unmodified bearing steel. Corresponding Miller indices for the ferrite phase (body centered cubic, bcc) and the austenite phase (face centered cubic, fcc) are indicated. (For interpretation of the references to colour in this figure legend, the reader is referred to the web version of this article.)

amounts of lubricants in a network of sharp-edged gaps (gap widths of 10–100 nm) thereby providing areal lubrication.

Altogether this permits rapid movements of steel ball counterbodies over the platelets ($2\ ms^{-1}$ in the present study) without tearing off the lubricant film. In this picture, both the friction and the wear behavior (Fig. 2c,d) become comprehensible: Surface modifications conducted with laser fluences of $F = 300\ Jcm^{-2}$ result in oxide platelets featuring comparably low thickness and low roughness (Fig. 1d,e).

Consequently, friction is initially low since the smooth topography enables unimpeded sliding. High susceptibility to mechanical damage, however, limits the overall performance once the coating is critically damaged. This behavior can be improved when the laser fluence applied for the generation of metal oxide platelets is slightly increased. Mechanical robustness is enhanced but also surface roughness thus yielding low or rather close to zero wear combined with still distinct reductions of friction. In contrast, laser fluences by far exceeding $1\ kJcm^{-2}$ result in metal oxide platelets featuring average thicknesses of 120 nm and $R_a = 0.25\mu m$. Such metal oxides act more and more abrasive against untreated 100Cr6 counterbodies thus tending to inflict systemically wear (see Supporting Information for details). Common to all types of metal oxide platelets is a strong adhesion to the steel substrates.

A detailed view at the interface responsible for this property is provided in Fig. 5a. Cross-sectional STEM imaging of 100Cr6 modified with $F = 1067\ Jcm^{-2}$ shows metal oxides featuring a columnar substructure. According to elemental analysis (EDX), iron oxide is the major component besides traces of manganese and chromium oxides. Moreover, a significant proportion of carbon is detected although 100Cr6 contains only about 1% carbon. Most notably, a carbon peak is localized in the interface between the metal oxides and the underlying steel substrate. X-ray diffraction analyses (Fig. 5b) prove, that laser modifications of 100Cr6 induce partial transformations of the predominant ferrite phase (bcc) to the austenite phase (fcc). Compared to ferrite, the carbon solubility of austenite is higher which explains the detected carbon peak in the subsurface zone. The flank of the carbon peak protrudes into the oxide layer thus implying that the interface between metal oxides and steel is enriched with carbon. Since X-ray diffractometry does not indicate the presence of carbides, it is concluded that this interface contains significant amounts of amorphous carbon or graphite. It is surmised that this carbon species acts as a solid lubricant that promotes the relocatability of metal oxide platelets thus enabling shape adaptions to plastic deformations of the steel substrate. This interpretation is supported by electron micrographs of individual platelets (Fig. 4e,f, and h). Nanorod arrays resembling the platelets are enveloped by a material imaged in green. With regard to material contrast, this material features strong similarities to an underlying carbon film (Fig. 4h) thus suggesting that it is indeed carbon, which, like carbon in general, acts as a dry lubricant. In this respect, the created system is comparable to scale armor and features similarities to natural materials such as nacre that comprises alternating layers of hard inorganic platelets and soft organic macromolecules whose interplay results in a unique combination of strength and toughness.

3. Conclusions

A facile laser treatment enhancing the tribological performance of standard bearing steel is reported in this work. The process is conducted in ambient air thus enabling easy integration in already existing production lines. Using the example of 100Cr6, a widely applied alloy for the manufacture of ball and roller bearings, the laser process facilitates friction reduction of 54% concomitant with close to zero wear. Even friction reductions up to 90% are possible; however, this can only be achieved at the price of low mechanical robustness. Nanostructured metal oxide plates are found to be responsible for this astonishing increase in tribological performance. The formation of metal oxide platelets, which represent arrays of vertically aligned nanorods, is based on self-organization or rather pulsed laser-induced dewetting (PLiD)

with simultaneous oxidation. Resulting nanorod arrays float on carbonaceous materials that act as a solid lubricant thus promoting shape adaptions to plastic deformations such as edges and scars induced by high mechanical stress. These metal oxides protect the steel surface similar to a scale armor. The hierarchical morphology of the platelets provides an ideal ground for the stabilization of lubricant films thus facilitating rapid movements (2 m/s) of counterbodies without tearing off the lubricating effect essential for high tribological performance.

Appendix A: Sample preparation

Hardened chromium steel type 100Cr6 (1.5% Cr, 1% C, 0.35% Mn, balance Fe), a standard material for the manufacture of roller bearings, was used as the base material for tribological investigations on the effect of laser modification. A 100Cr6 plate of 2.5 mm thickness was cut into samples of 20×20 mm edge length which were equipped with rounded edges and a center hole of 10 mm diameter in order to fit the dimensional requirements of the ball-on-disk machine. Prior to laser-treatment, the samples were polished to a surface roughness of $R_a = 0.02 - 0.03\mu m$.

Laser modifications of 100Cr6 samples were carried out in ambient air using a frequency doubled nanosecond pulsed laser (Spectra Physics Explorer XP 5–532, Newport, USA) emitting a wavelength of 532 nm. All samples were irradiated at an average laser power of 1.6 W, a pulse frequency of 50 kHz, a pulse energy of 32 μJ, and a pulse width of 6 ns. The laser beam was focused to a spot diameter of 30 μm ($1e^{-2}$) by an F-Theta lens (Rhodenstock 163–532, Germany) with a focal length of 163 mm and scanned over the 100Cr6 samples using a galvanometer scan head (ScanGine 14, Scanlab, Germany). Each steel sample in the set was subjected to a specific laser fluence F by variations of the line scan speed while the line spacing was kept constant at 3 μm. Using this setup, scan speeds S corresponding to respective laser fluences F are as follows: $S = 800$ mm/s, $F = 67\ Jcm^{-2}$; $S = 600$ mm/s, $F = 89\ Jcm^{-2}$; $S = 400$ mm/s, $F = 133\ Jcm^{-2}$; $S = 200$ mm/s, $F = 267\ Jcm^{-2}$; $S = 100$ mm/s, $F = 533\ Jcm^{-2}$; $S = 50$ mm/s, $F = 1067\ Jcm^{-2}$; $S = 25$ mm/s, $F = 2134\ Jcm^{-2}$; $S = 12.5$ mm/s, $F = 4268\ Jcm^{-2}$; $S = 6.25$ mm/s, $F = 8535\ Jcm^{-2}$.

Appendix B: Tribological analysis

For tribological evaluation, a pin-on-disk tribometer was used which is described in detail in a previous publication[11]. The tribometer is operated in the same way as a typical pin on disk tribometer but with a fixed 100Cr6-steel ball used as pin or rather counterbody. The 100Cr6 ball was rotated over test samples in a circular movement resulting in sliding friction with a slip rate of 100%, which means there was no rolling motion of the 100Cr6 ball. All measurements have been carried out in an oil bath (Castrol X320) at a constant temperature of 70 °C. The friction between 100Cr6 steel balls and respective substrates was measured by recording the current of the electric motor while a feedback electronic kept the rotational speed constant. After each measurement, the viscous friction related to the movement of the steel ball and the ball-mount in the oil bath has been measured separately and was subtracted from the overall friction signal in order to separate the friction contribution originating from the interface between the respective pairs of steel ball and sample [11]. Full tribological records of the sample set are provided in the Supporting Information.

Appendix C: Surface analysis, TEM, and EDX

The surface roughness of 100Cr6 samples was determined with a VK9710 scanning laser microscopy (Keyence, Japan) at 50-fold magnification. Scanning electron microscopy (SEM) was performed on a field emission microscope (JSM-7500F, Jeol, Japan) equipped with back-scattered electron detector (YAG, Autrata, Czech Republic) for material contrast imaging based on effective atomic number contrast Zeff. The total abrasion volumes of 100Cr6 samples subjected to ball-on-disk examinations were determined from surface profiles recorded with white light interferometry WLI (CT 100, Cyber Technologies, Germany). For the different steps of this non-standard procedure, please see the Supporting Information for details. The cross-sectional inspection of laser modified 100Cr6 was performed on a Scios 2 focused ion beam (FIB)-SEM (Thermo Fischer Scientific, USA) via lamella preparation and subsequent STEM imaging (scanning transmission electron microscopy at 30 kV) and energy dispersive X-ray spectrometry (EDX). Crystal structure analysis was performed on an X'pert PRO MPD (Philips, Netherlands) X-ray powder diffractometer (XPD) equipped with an X'pert tube Co LFF operating at 40 kV and 30 mA. Diffractograms were recorded in a range of $45° \leq 2\Theta \leq 105°$ in an angular resolution of $0.1°2\Theta$ at room temperature.

Appendix D. Supporting information

Supplementary data associated with this article can be found in the online version at doi:10.1016/j.triboint.2021.107138.

References

[1] Holmberg K, Erdemir A. Influence of tribology on global energy consumption, costs and emissions. Friction 2017;5:263–84. https://doi.org/10.1007/s40544-017-0183-5.

[2] Zhang S-W. Green tribology: fundamentals and future development. Friction 2013; 1:186–94. https://doi.org/10.1007/s40544-013-0012-4.

[3] M., Nosonovsky, B., Bhushan (Eds.), Green Tribology: Biomimetics, Energy Conservation and Sustainability, Green Energy and Technology, Springer-Verlag, Berlin Heidelberg, (2012). ⟨https://www.springer.com/de/book/978364223 6808⟩.

[4] Spikes H. The history and mechanisms of ZDDP. Tribol Lett 2004;17:469–89.

[5] Gosvami NN, Bares JA, Mangolini F, Konicek AR, Yablon DG, Carpick RW. Mechanisms of antiwear tribofilm growth revealed in situ by single-asperity sliding contacts. Science 2015;348:102–6. https://doi.org/10.1126/science.1258788.

[6] Spikes H. Friction modifier additives. Tribol Lett 2015;60:5. https://doi.org/10.1007/s11249-015-0589-z.

[7] Berman D, Deshmukh SA, Sankaranarayanan SKRS, Erdemir A, Sumant AV. Macroscale superlubricityenabled by graphene nanoscroll formation. Science 2015. https://doi.org/10.1126/science.1262024. http://www.sciencemag.org/cgi/doi/10.1126/science.1262024.

[8] Du P, Chen G, Song S, Chen H, Li J, Shao Y. Tribological properties of muscovite, CeO₂ and their composite particles as lubricant additives. Tribol Lett 2016;62:29.

[9] Zhao F, Bai Z, Fu Y, Zhao D, Yan C. Tribological properties of serpentine, La(OH)₃ and their composite particles as lubricant additives. Wear 2012;288:72–7. https://doi.org/10.1016/j.wear.2012.02.009.

[10] Bucholz EW, Zhao X, Sinnott SB, Perry SS. Friction and wear of pyrophyllite on the atomic scale. Tribol Lett 2012;46:159–65. https://doi.org/10.1007/s11249-012-9927-6.

[11] Chizhik P, Dietzel D, Bill S, Schirmeisen A. Tribological properties of a phyllosilicate based microparticle oil additive. Wear 2019;426–427:835–44. https://doi.org/10.1016/j.wear.2019.01.118. ⟨http://www.sciencedirect.com/science/article/pii/S0043164819302017⟩.

[12] Gupta B, Kumar N, Panda K, Dash S, Tyagi AK. Energy efficient reduced graphene oxide additives: mechanism of effective lubrication and antiwear properties. Sci Rep 2016;6:18372. https://doi.org/10.1038/srep18372. ⟨https://www.nature.com/articles/srep18372⟩.

[13] Berman D, Erdemir A, Sumant AV. Graphene: a new emerging lubricant. Mater Today 2014;17:31–42. https://doi.org/10.1016/j.mattod.2013.12.003. ⟨http://www.sciencedirect.com/science/article/pii/S1369702113004574⟩.

[14] Berman D, Erdemir A, Sumant AV. Few layer graphene to reduce wear and friction on sliding steel surfaces. Carbon 2013;54:454–9. https://doi.org/10.1016/j.carbon.2012.11.061. ⟨http://linkinghub.elsevier.com/retrieve/pii/S000862231 2009529⟩.

[15] Koren E, Lörtscher E, Rawlings C, Knoll AW, Duerig U. Adhesion and friction in mesoscopic graphite contacts. Science 2015;348:679–83. https://doi.org/10.1126/science.aaa4157. ⟨http://www.sciencemag.org/content/348/6235/679⟩.

[16] Li J, Zhang C, Ma L, Liu Y, Luo J. Superlubricity achieved with mixtures of acids and glycerol. Langmuir 2013;29:271–5. https://doi.org/10.1021/la3046115.

[17] Baykara MZ, Vazirisereshk MR, Martini A. Emerging superlubricity: a review of the state of the art and perspectives on future research. Appl Phys Rev 2018;5:041102. https://doi.org/10.1063/1.5051445. ⟨http://aip.scitation.org/doi/10.1063/1.5051445⟩.

[18] Erdemir A. The role of hydrogen in tribological properties of diamond-like carbon films. Surf Coat Technol 2001;146–147:292–7. https://doi.org/10.1016/S0257-8972(01)01417-7. ⟨http://www.sciencedirect.com/science/article/pii/S025789 7201014177⟩.

[19] Erdemir A, Donnet C. Tribology of diamond-like carbon films: recent progress and future prospects. J Phys D Appl Phys 2006;39:R311–27. https://doi.org/10.1088/0022-3727/39/18/R01. ⟨http://stacks.iop.org/0022-3727/39/i=18/a=R01?ke y=crossref.9af827cc7f4ea226ffcf654a7b79e6d5⟩.

[20] Kalin M, Vizintin J. A comparison of the tribological behaviour of steel/steel, steel/DLC and DLC/DLC contacts when lubricated with mineral and biodegradable oils. Wear 2006;261:22–31. https://doi.org/10.1016/j.wear.2005.09.006. ⟨http://www.sciencedirect.com/science/article/pii/S0043164805004540⟩.

[21] Ronkainen H, Varjus S, Holmberg K. Friction and wear properties in dry, water- and oil-lubricated DLC against alumina and DLC against steel contacts. Wear 1998; 222:120–8. https://doi.org/10.1016/S0043-1648(98)00314-7. ⟨http://www.sciencedirect.com/science/article/pii/S0043164898003147⟩.

[22] Tasdemir HA, Tokoroyama T, Kousaka H, Umehara N, Mabuchi Y. Friction and wear performance of boundary-lubricated DLC/DLC contacts in synthetic base oil. Procedia Eng 2013;68:518–24. https://doi.org/10.1016/j.proeng.2013.12.215. ⟨http://www.sciencedirect.com/science/article/pii/S1877705813020699⟩.

[23] Erdemir A. Genesis of superlow friction and wear in diamondlike carbon films. Tribol Int 2004;37:1005–12. https://doi.org/10.1016/j.triboint.2004.07.018. ⟨http://www.sciencedirect.com/science/article/pii/S0301679×04001367⟩.

[24] Erdemir A, Eryilmaz OL, Fenske G. Synthesis of diamondlike carbon films with superlow friction and wear properties. J Vac Sci Technol A 2000;18:1987–92. https://doi.org/10.1116/1.582459. ⟨https://avs.scitation.org/doi/10.1116/1.582459⟩.

[25] Fotovvati B, Namdari N, Dehghanghadikolaei A. On coating techniques for surface protection: a review. J Manuf Mater Process 2019;3:28. https://doi.org/10.3390/jmmp3010028. ⟨https://www.mdpi.com/2504-4494/3/1/28⟩.

[26] Shen C, Khonsari MM. The effect of laser machined pockets on the lubrication of piston ring prototypes. Tribol Int 2016;101:273–83. https://doi.org/10.1016/j.triboint.2016.04.009. ⟨https://www.sciencedirect.com/science/article/pii/S0301679×1630055X⟩.

[27] Voevodin AA, Zabinski JS. Laser surface texturing for adaptive solid lubrication. Wear 2006;261:1285–92. https://doi.org/10.1016/j.wear.2006.03.013. ⟨https://www.sciencedirect.com/science/article/pii/S0043164806001335⟩.

[28] Zhao Q-Z, Wang Z. Manipulation of tribological properties of metals by ultrashort pulsed laser micro-/nanostructuring. Adv Tribol 2016. https://doi.org/10.5772/64764. https://www.intechopen.com/books/advances-in-tribology/manipulation-of-tribological-properties-of-metals-by-ultrashort-pulsed-laser-micro-nanostructuring.

[29] Kasem H, Stav O, Grützmacher P, Gachot C. Effect of low depth surface texturing on friction reduction in lubricated sliding contact. Lubricants 2018;6:62. https://doi.org/10.3390/lubricants6030062. ⟨https://www.mdpi.com/2075-4442/6/3/62⟩.

[30] Fowell MT, Medina S, Olver AV, Spikes HA, Pegg IG. Parametric study of texturing in convergent bearings. Tribol Int 2012;Complete:7–16. https://doi.org/10.1016/j.triboint.2012.02.013. ⟨https://www.infona.pl/resource/bwmeta1.element.elsevier-8fdad8a5-eadb-3717-a312-e44e040d934c⟩.

[31] Rosenkranz A, Heib T, Gachot C, Mücklich F. Oil film lifetime and wear particle analysis of laser-patterned stainless steel surfaces. Wear 2015;334–335:1–12. https://doi.org/10.1016/j.wear.2015.04.006. ⟨http://www.sciencedirect.com/science/article/pii/S0043164815002045⟩.

[32] Andersson P, Koskinen J, Varjus S, Gerbig Y, Haefke H, Georgiou S, et al. Microlubrication effect by laser-textured steel surfaces. Wear 2007;262:369–79. https://doi.org/10.1016/j.wear.2006.06.003. ⟨https://linkinghub.elsevier.com/retrieve/pii/S0043164806002572⟩.

[33] Dumitru G, Romano V, Weber H, Haefke H, Gerbig Y, Pflüger E. Laser microstructuring of steel surfaces for tribological applications. Appl Phys A 2000; 70:485–7. https://doi.org/10.1007/s003390051073. ⟨https://doi.org/10.1007/s003390051073⟩.

[34] Jervis TR, Hirvonen JP. Tribology and surface mechanical properties of the oxide film formed by excimer laser surface treatment of AISI 304 stainless steel. Wear 1991;150:259–65. https://doi.org/10.1016/0043-1648(91)90321-K. ⟨https://www.sciencedirect.com/science/article/pii/004316489190321K⟩.

[35] Batchelor AW, Stachowiak GW, Cameron A. The relationship between oxide films and the wear of steels. Wear 1986;113:203–23. https://doi.org/10.1016/0043-1648(86)90121-3. ⟨http://www.sciencedirect.com/science/article/pii/0043164886901213⟩.

[36] T.R. Jervis, M. Nastasi, A.J. Griffin, T.G. Zocco, T.N. Taylor, S.R. Foltyn, Excimer laser processing of tool steel: tribological effects of multiple pulse processing and Ti alloying, MRS Online Proceedings Library Archive 397 (1995).10.1557/PROC-397 –531.⟨https://www.cambridge.org/core/journals/mrs-online-proceedings-library-archive/article/excimer-laser-processing-of-tool-steel-tribological-effects-of-multiple-pulse-processing-and-ti-alloying/BD7CF53CADC26FD16FBEC51BC3A06D70⟩.

[37] Reinhardt H, Pietzonka C, Harbrecht B, Hampp N. Laser-directed self-organization and reaction control incomplex systems: a facile synthesis route for functional materials. Adv Mater Interfaces 2014;1. https://doi.org/10.1002/admi.201300060. http://onlinelibrary.wiley.com/doi/10.1002/admi.201300060/abstract.

[38] Chizhik P, Friedrichs M, Dietzel D, Schirmeisen A. Tribological analysis of contacts between glass and tungsten carbide near the glass transition temperature. Tribol Lett 2020;68:127. https://doi.org/10.1007/s11249-020-01363-0. ⟨http://link.springer.com/10.1007/s11249-020-01363-0⟩.